

Multipartite entanglement structures in quantum stabilizer states

Vaibhav Sharma* and Erich J Mueller†

Laboratory of Atomic and Solid State Physics, Cornell University, Ithaca, New York

(Dated: November 6, 2024)

We develop a method for visualizing the internal structure of multipartite entanglement in pure stabilizer states. Our algorithm graphically organizes the many-body correlations in a hierarchical structure. This provides a rich taxonomy from which one can extract a number of traditional quantities such as entanglement depth and entanglement entropy. Our construction is gauge invariant and goes beyond traditional entanglement measures by visually revealing how quantum information and entanglement is distributed. We use this tool to analyze the internal structures of prototypical stabilizer states (GHZ state, cluster state, stabilizer error correction codes) and are able to contrast the complexity of highly entangled volume law states generated by random unitary operators and random projective measurements.

I. INTRODUCTION

Entanglement is the key feature that distinguishes quantum and classical systems. It is a valuable resource for quantum information processing and computation [1]. When restricted to two parties, entanglement is well understood: Bipartite entanglement measures are very intuitive, and there is no controversy about how to detect or quantify two-particle entanglement. For many-body systems, the situation is different. Characterizing and understanding multipartite entanglement is challenging due to its far richer structure that cannot be easily summarized [2]. Here we develop a more intuitive and broadly applicable approach towards organizing and visualizing multipartite entanglement in stabilizer states.

There exist several measures of multipartite entanglement such as the entanglement entropy [3], entanglement depth [4, 5], global entanglement [6], quantum Fisher information [7], Schmidt measure [8], generalized geometric measure [9] and N-tangle [10]. Each of these measures emphasize a different aspect of multipartite entanglement, quantifying it with a single number. Although they provide useful information, they fail to fully capture the complexity of a multipartite entangled state, such as the internal structure of correlations and the local distribution of entanglement. This is especially apparent for states that are not described by traditional order parameters, such as those generated by noisy quantum circuits. In this work, our goal is to resolve the structure of an entangled state and develop a way to visualize multipartite entanglement, going beyond reducing it to a single numerical quantity. We propose organizing multipartite entanglement via the topological structure of correlations present in the state. We group the qubits in a quantum state in clusters characterized by a parameter, w . The defining features of these w -clusters is that each qubit inside them has non-zero mutual information with a subset

of least $(w-1)$ other qubits within the same cluster. The idea is that w qubits together encode information that is not present in any individual qubit. We then recursively continue to group these clusters together, forming an entanglement structure diagram that shows how various parts of the system are connected. There is some relationship between this concept and the idea of the *information lattice*, which additionally incorporates spatial information [11–13].

Following this approach, we are able to directly visualize how quantum information is spread throughout the system in highly-entangled states. We get access to the internal structure of correlations that connect various qubits in a composite many-body state. We note that the recursive nature of our method makes extracting such information much more efficient than simply calculating bipartite entanglement entropy across all possible partitions of a given system. Our method also provides the entanglement depth and can be used to bound entanglement entropies.

We illustrate our decomposition by looking at well-known stabilizer states: the cluster state, GHZ state and the logical states of error correction codes such as the 5-qubit code and the 7-qubit CSS code. The true power of our construction, however, is revealed by looking at highly entangled volume law states generated by random two-qubit Clifford unitaries and random three-qubit projective measurements [14, 15]. Although both sets of states show volume law scaling of bipartite entanglement entropy, we find that the entanglement structure diagrams are able to distinguish between them.

II. ALGEBRAIC STRUCTURE

Our approach works for stabilizer states [16], which are an important class of quantum states which are used in quantum computing and play an important role in quantum error correction. An N qubit stabilizer state is the simultaneous eigenstate of N linearly independent commuting Pauli strings, referred to as the stabilizer generators. For example, the cat state, $1/\sqrt{2}(|111\rangle + |000\rangle)$ is the simultaneous eigenstate of three Pauli string opera-

* vaibhavsharma@rice.edu; Current Address: Department of Physics, Rice University, Houston, Texas

† em256@cornell.edu

tors, $Z_1Z_2I_3$, $I_1Z_2Z_3$ and $X_1X_2X_3$. Trivially, a stabilizer state is also an eigenstate of any member of the *stabilizer group* formed by taking arbitrary products of the generators. The stabilizer generators are not unique, and can be replaced by any N linearly independent elements of the stabilizer group. This freedom to choose the generators is often referred to as a *gauge* freedom. We only consider *pure* quantum states, and will not discuss the properties of ensembles encoded by density matrices.

A generic Pauli string can be written as $P = \prod_j X_j^{\alpha_j} Z_j^{\beta_j}$, where $\alpha_j, \beta_j = 0, 1$. The *support* of a Pauli string is the set of qubits for which α and/or β is non-zero. The *weight* of the string is the number of qubits in the support. The expectation value of a weight- w stabilizer can be interpreted as the expectation value of a w -spin correlation function. In our approach, we recursively group sets of qubits into clusters. At each iteration, we take the weight of a stabilizer to be the number of clusters in its support, rather than the number of qubits.

A key feature of stabilizer states is that the bipartite entanglement entropy is *quantized*. If we break a stabilizer state into two disjoint sets of qubits, the entanglement entropy across the cut is always a multiple of $\ln(2)$. If region A contains n_A qubits then $S_A \leq n_A \ln(2)$. When this bound is saturated, we refer to A as being *maximally entangled*. One learns nothing about the state of the system by interrogating region A . There is no information which is exclusively stored in A , and the reduced density matrix is the identity matrix of dimension 2^{n_A} .

A useful intuition is that if $S_A = s_a \ln(2)$ with respect to the rest of the system, then there are $n_A - s_a$ bits of information that are locally stored within A . In particular, it is an eigenstate of exactly $n_A - s_a$ linearly independent Pauli strings whose support is entirely within A . These are the operators which measure the stored information. They generate a subgroup of the stabilizer group, which we refer to as the A -stabilizers. Another useful feature is that the reduced density matrix of A has rank 2^{s_a} .

We can generalize this notion to the case when region A is divided into disjoint clusters of qubits, constructed by some as-yet unspecified algorithm. Each cluster will be labeled by an index i . Following Watanabe [17], we define the *total correlations* in A to be $I_A = (\sum_{i \in A} S_i) - S_A$ where S_i is the entanglement entropy of cluster i with the rest of the system. The total correlations are also referred to as the “multipartite quantum mutual information” [18]. It tells us how many bits of information are stored in A , but which are not stored solely by any single cluster within A .

We now coin three new terms: *w-indivisible*, *w-connected* and *w-cluster*. We say that region A is *w-indivisible* if any subset $C \subset A$ containing $w - 1$ or fewer elements have vanishing total correlations, $I_C = 0$. Equivalently, any stabilizers whose support lies solely in A must have a weight greater or equal to w .

We say that A is *w-connected* if every element $j \in A$ belongs to a set $B \subseteq A$ containing w elements, such that B has non-zero total correlations. Furthermore, B cannot

be disjoint from all other such w -element subsets within A . Equivalently, every element of A is in the support of an A -stabilizer of weight less than or equal to w . The region A is a *w-cluster* if it is both *w-indivisible* and *w-connected*.

In our construction, we use an iterative method to divide the system into w -clusters. In the first iteration, each qubit is considered as a single element. At each subsequent iteration, any w -clusters found in the previous iteration are treated as single indivisible elements. We begin by finding all of the qubits which are disentangled from the rest of the system. These are 1-clusters. These singletons are decoupled from the rest of the system and can be ignored at future steps. Next we find all of the qubits which belong to 2-clusters. Formally these can be found by constructing all stabilizers of weight 2, or by looking at the reduced density matrix for each pair. The sets of elements which are connected by these stabilizers form the 2-clusters. At this point we treat the clusters as indivisible elements. We then repeat the previous steps – removing single elements which are decoupled, and forming new 2-clusters of the given elements. We iterate until no new 2-clusters can be formed. We then search for 3-clusters, if there are any elements which have not yet been assigned to decoupled clusters. If any 3-clusters are found, we repeat all the previous steps. We always construct as many low weight clusters as possible before moving on to higher weight clusters. This procedure can be repeated with 4-clusters, 5-clusters... until all qubits have been assigned to large decoupled clusters. We give more details of the computational procedure in Appendix A.

A short example is useful. Consider the 4-qubit state, $|\psi\rangle$ with stabilizer generators Z_1Z_2 , Z_3Z_4 , $X_1X_2Z_3$ and $Z_2X_3X_4$. Up to a normalization constant, $|\psi\rangle = |1111\rangle + |0011\rangle + |1100\rangle - |0000\rangle$. The entanglement structure of this state is shown in Fig. 1. Here the qubits are labeled by black integers. The w -clusters are denoted by ovals, with w shown in red. In the first round, our algorithm produces two 2-clusters: (1, 2) and (3, 4). In the second round, we consider the clusters (1, 2) and (3, 4) as single indivisible elements. We then see that these together form one large 2-cluster: ((1, 2), (3, 4)) connecting all four qubits into a single many-body state. Such a structure implies that while qubits 1, 2 and 3, 4 are directly connected by weight-2 stabilizers, qubits 1, 3 and qubits 1, 4 are only connected by higher weight stabilizers. In this way our construction recursively forms clusters to build a complete description of entanglement within the many-body state.

Fig. 2 shows a more complicated entanglement structure diagram of a 16-qubit state. In this diagram, qubit 16 forms an isolated cluster. This means that it is not entangled with any other qubit. Qubits labeled 13, 14 and 15 similarly form an independent cluster which is unentangled with the rest of the system. It is labeled as a 2-cluster, indicating that each of these qubits must be in the support of a weight 2 stabilizer, whose support

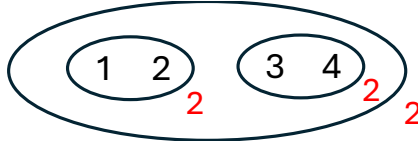


FIG. 1. Entanglement structure diagram of a four qubit state given by the wavefunction, $|\psi\rangle = 1/2(|1111\rangle + |0011\rangle + |1100\rangle - |0000\rangle)$. The qubits, labeled by black integers, are placed in clusters denoted by drawing circles around them. The clusters are then considered indivisible entities and can be further placed into bigger clusters. The small red number, w in the bottom left of a clustering circle denotes that the entities inside that cluster share a minimum of w -point correlation function among the entities.

is fully within this cluster. Up to local Pauli rotations, an unentangled 2-cluster of three spins is a GHZ state $|111\rangle + |000\rangle$.

The middle cluster containing qubits from 1-12 is the largest, with multiple sub-clusters. At the first level, qubits (1,4), qubits (2,3) and qubits (5,12) are placed in 2-clusters, denoting presence of weight 2 stabilizers. By virtue of being 2-clusters that are not isolated, each of them contains one bit of information and has an entanglement entropy $S = \ln 2$ with the rest of the system.

In the next iteration, the 2-clusters formed by qubits (1,4) and qubits (2,3) join together to form a bigger 2-cluster. There is a stabilizer whose support is in both of these clusters but that cannot be individually confined to either one of these. Similarly, the 2-cluster of qubits (5,12) joins with qubit 6 to form a bigger 2-cluster.

We can further deduce constraints from the fact that (1,4) and (2,3) are 2-clusters embedded in a larger 2-cluster. There is a stabilizer whose support lies in (1,2,3,4). It must have support on at least 3 of these qubits – as otherwise (1,2,3,4) would have all been placed in one 2-cluster during the first iteration.

In the next iteration, the clusters of qubits ((1,4),(2,3)) and qubits (5,6,12) further join to form a new 2-cluster. At the final level, this newly formed cluster joins with the 5 individual qubits labeled from 7-11 in a 3-cluster to form a big independent cluster containing qubits 1-12. This is labeled a 3-cluster, meaning that any of the elements can be joined up with two others to form a set which contains the support of a stabilizer.

A. Entanglement depth

Having constructed an entanglement diagram, we can readily extract the *entanglement depth* [4, 5]. Any n -qubit pure state can be written as a product state over m disjoint regions in the following form,

$$|\psi\rangle = |\phi_1\rangle_{A_1} \otimes |\phi_2\rangle_{A_2} \dots \otimes |\phi_m\rangle_{A_m} \quad (1)$$

where none of the $|\phi_j\rangle_{A_j}$ can be further decomposed into product states. If there are at most k qubits in any of the

m regions, the state is deemed to have an entanglement depth of k [4, 5]. The state is said to have k -qubit multiparticle entanglement. In our entanglement structure diagram, the entanglement depth is simply the number of qubits in the largest cluster.

In the four qubit example shown in Fig. 1, all the qubits are ultimately part of one big cluster, denoting an entanglement depth of 4. In contrast, the diagram in Fig. 2 shows that the 16-qubit state can be written as a product state of the form, $|\psi\rangle = |\phi_1\rangle_{A_1} \otimes |\phi_2\rangle_{A_2} \otimes |\phi_3\rangle_{A_3}$ where region A_1 contains qubits labeled from 1-12, A_2 contains qubits 13-15 and A_3 contains the qubit 16. Clearly this state has an entanglement depth of 12.

B. Minimal stabilizer weight

Another important feature that can be extracted from these diagrams is the weight of the smallest stabilizer in the stabilizer group. We refer to this as the *minimal stabilizer weight*. It reveals the degree of delocalization of the quantum information. In the entanglement diagram, one can identify the minimal stabilizer weight as the smallest w , for the w -clusters in the first iteration of our algorithm.

C. Bipartite entanglement entropy

We can also use the diagram to obtain an upper bound on the bipartite entanglement entropy across any given partition. Consider a set of n qubits that are partitioned into two regions, region A containing m and region B containing $n - m$ qubits with $m < n - m$. The maximum entanglement entropy across the partition in a stabilizer state is $m \ln 2$ since there are only m units of information available in region A that can be shared with the other region B . Within region A , any local clusters consisting of qubits entirely within the region reduce the entanglement entropy across the partition by at-least one unit. This is because such a local cluster denotes a stabilizer that is completely confined within the region A . Identifying such local clusters gives upper bounds to the entanglement entropy of a given region with the rest of the system.

The four qubit example of Fig. 1 is the easiest to understand. Consider region A with qubits (1, 2) and region B with qubits (3, 4). Simply by counting the number of qubits we know that the maximum possible bipartite entanglement entropy between A and B is $2 \ln 2$. Beyond that, within region A there is one local cluster containing one unit of information entirely within A . This reduces the entanglement entropy across the partition by $\ln 2$. Thus we know that the entanglement entropy across the partition is bounded from above by $\ln 2$. In this case the bound is saturated, as the two subclusters belong to one bigger cluster, and hence share one bit of information.

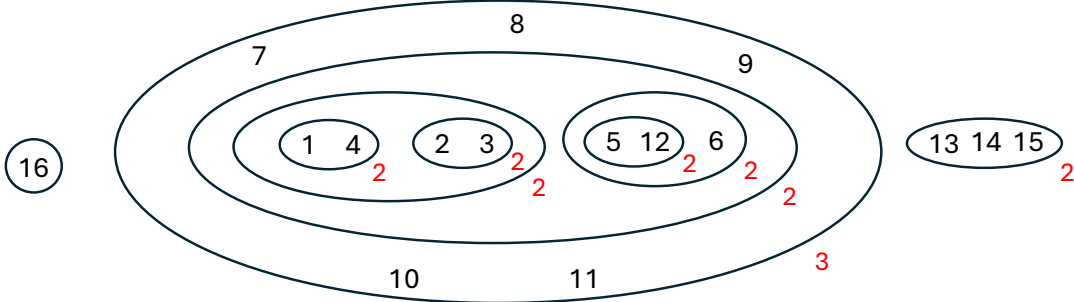


FIG. 2. An entanglement structure diagram of an arbitrary 16 qubit stabilizer state is shown. The state is separable with qubits labeled 1-12 forming the largest cluster, corresponding to an entanglement depth of 12. The nested structure of the clusters shows how correlations are distributed in the state.

Now consider the example shown in Fig. 2, where qubits 1-12 are in a pure state. We can separate that pure state into two regions – for example, we take region A to contain qubits 1-6 and region B to contain qubits 7-12. From counting qubits, the maximum possible entanglement entropy across this partition is $6 \ln 2$. Within region A , we see two sub-clusters that are 2-clusters containing qubits (1,4) and qubits (2,3). They reduce the entanglement entropy across the partition by $2 \ln 2$. They are both further joined in another local 2-cluster, reducing the entropy further by $\ln 2$. Thus the upper bound on entanglement entropy between regions A and B is $3 \ln 2$.

III. ENTANGLEMENT STRUCTURES OF SOME PROTOTYPICAL STATES

We can use the entanglement structure diagrams to visualize some prototypical stabilizer states. The diagram for a GHZ state [19] of 8 qubits, $|\psi\rangle = 1/\sqrt{2}(|11111111\rangle + |00000000\rangle)$ is shown in Fig. 3(a). Among the eight stabilizer generators of the GHZ state, seven can be taken to have the form, $S_i = Z_i Z_{i+1}$ where $i \in [1, \dots, 7]$. The eighth generator can be chosen to be $S_8 = X_1 X_2 \dots X_8$. Here Z_i, X_i are Pauli operators σ_i^z, σ_i^x for the qubit labeled i . All the qubits share one big 2-cluster, denoting the presence of 2-point correlations (weight-2 stabilizers) and a full entanglement depth of 8. In fact, in a GHZ state, each qubit pair (i,j) is in the support of a weight two stabilizer, $Z_i Z_j$.

In Fig. 3(b) we show the entanglement structure diagram for the 8-qubit cluster state on a 1D lattice without periodic boundary conditions [20]. This is defined by its stabilizer generators: $S_j = Z_{j-1} X_j Z_{j+1}$ for $j \neq 1, 8$ and $S_1 = X_1 Z_2, S_8 = Z_7 X_8$. These latter 2 generators have weight 2, and hence both (1,2) and (7,8) are placed in 2-clusters. Treating these 2-clusters as indivisible, the remaining stabilizers have the same topological structure. Thus ((1,2),3) and (6,(7,8)) form 2 clusters. We can repeat, until one large cluster is formed. The local nature of the correlations is apparent in the nested clusters. As with the GHZ state, the entanglement depth is 8.

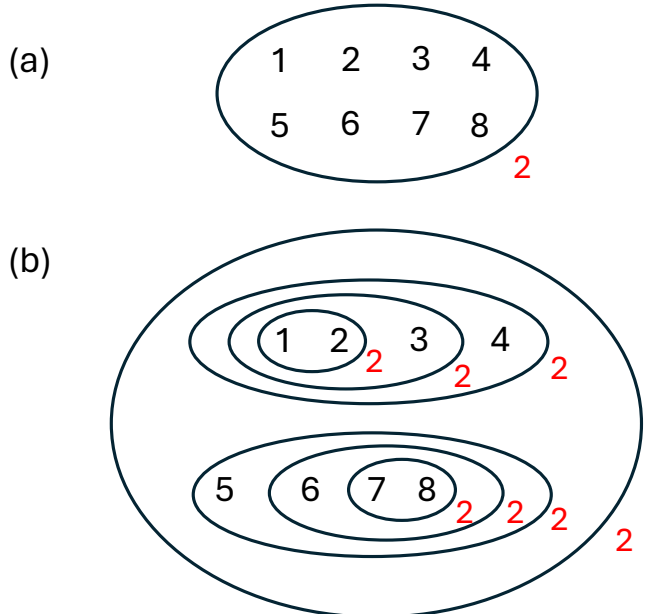


FIG. 3. Entanglement structure diagram of (a) 8-qubit GHZ state and (b) 8-qubit cluster state in 1D without periodic boundary conditions

Both the GHZ and the cluster state are low entanglement area law states. We know that across a bipartition in the center, they only have $\ln(2)$ entanglement entropy yet the entanglement diagrams have very different structures. The $\ln(2)$ entanglement of the cluster state can be extracted from the reasoning in Sec. II C. We imagine a bipartition into the regions $A = (1, 2, 3, 4)$ and $B = (5, 6, 7, 8)$. We can iteratively find the total correlations of region A : There is one bit of information stored in (1,2). Every time we grow that cluster, we add one qubit, but also add one confined stabilizer. Hence ((1,2),3) and (((1,2),3),4) each contain one bit of information. Consequently the bipartition into A and B has an entanglement entropy of only $\ln(2)$. The entanglement entropy of the GHZ state, however, cannot be extracted

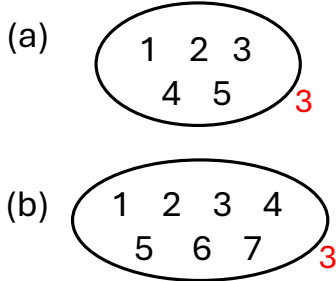


FIG. 4. Entanglement structure diagram of (a) the five-qubit error correcting code and (b) seven-qubit Steane CSS error correcting code

solely from the entanglement structure diagram.

Fig. 4(a),(b) show the entanglement structure diagrams of the five-qubit and seven-qubit error correcting codes. The stabilizer generators are given in Ref. [16] and these codes can correct arbitrary single qubit errors. The figures show the diagrams in the case when the logical qubit is in the eigenstate of the logical X operator. In both cases, all the qubits are in one 3-cluster showing an entanglement depth of 5 and 7 respectively. We can conclude that each of the qubits is in support of a weight 3 stabilizer that can be used to interrogate whether the system is in the code space. No extra information is given by the entanglement diagram, and one can argue that these diagrams have limited utility for such a class of states.

IV. ENTANGLEMENT STRUCTURES OF HIGHLY ENTANGLED VOLUME LAW STATES

We now analyze the internal structure of highly entangled volume law states generated in random quantum circuits. Random quantum circuits have recently been instrumental in enhancing our understanding of generic quantum dynamics and novel entanglement phase transitions [21]. In 1D systems, an entanglement phase transition between area law and volume law phases occurs when single site projective measurements are interspersed with random two-qubit unitary operators [14, 22–24]. Furthermore, there have been various measurement-only phase transitions from volume law to area law [15] or between different area law phases using random non-commuting projective measurements [25–31]. The states generated by typical random quantum circuits do not have an order parameter and are characterized by the scaling of their bipartite entanglement entropy. Not much is known about their spatial structure or properties. The entanglement structure diagrams can fill this gap.

We focus on volume law states in 1D generated by random local two-qubit Clifford unitary gates or random local three-qubit projective measurements. We take these

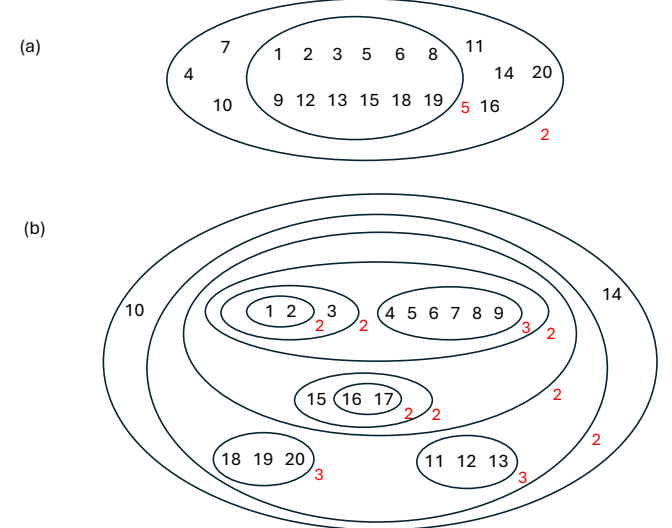


FIG. 5. Entanglement structure diagram of a typical 20 qubit volume law state generated by (a) local two-qubit random Clifford unitary gates and (b) local three-qubit random projective measurements

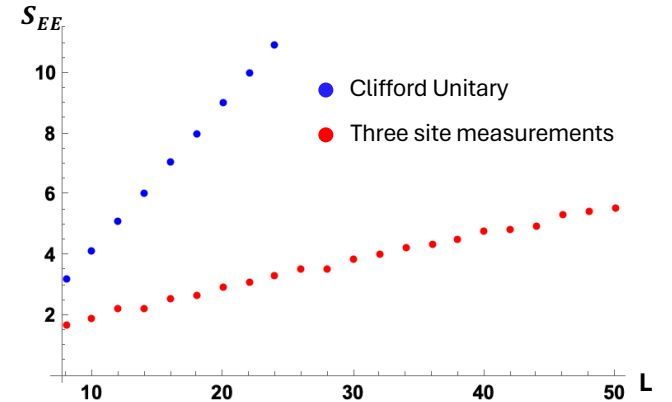


FIG. 6. Average bipartite entanglement entropy, S_{EE} as a function of system size L for states generated by two-qubit random Clifford unitary operators (blue) and three-qubit random measurements (red). S_{EE} scales linearly with L in both cases.

measurements to be random weight-3 Pauli strings acting on neighboring sites. In our analysis, we start from a product state and apply our random unitary gates or measurements until a steady state distribution is produced. We generate 500 states in both categories for various system sizes, L . In Fig. 6, we plot the average bipartite entanglement entropy, S_{EE} between two halves of the system as a function of system size L . In both cases, $S_{EE} \propto L$, signalling a volume law. For the same system sizes, S_{EE} is greater for the unitarily evolved state. In fact, the states generated by unitary evolution typically saturate S_{EE} such that, $S_{EE} \sim L/2$. These are referred to as Page states [32]. This maximal entanglement entropy reflects the behavior of a quantum state

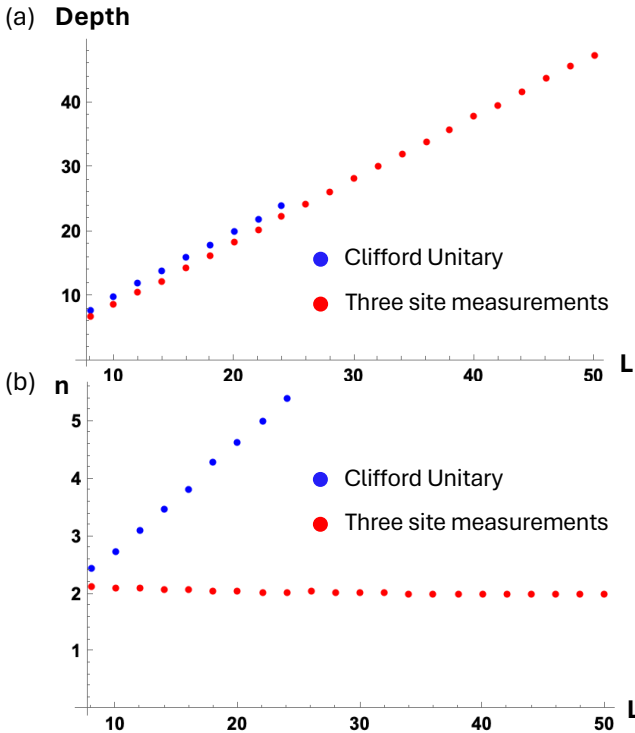


FIG. 7. (a) Average entanglement depth and (b) minimal stabilizer weight n of volume law states generated by two-qubit random Clifford unitary operators (blue) and three-qubit random measurements (red). Both kinds of volume law states have similar entanglement depth. However the minimal stabilizer weight found in the entanglement structure diagram scales linearly for unitarily evolved states while it remains constant for measurement-only states

under chaotic evolution where the quantum information is maximally scrambled. In contrast, the states generated purely by measurements have a lower entanglement entropy, but still follow the volume law. We will see how the entanglement structure diagrams can help us to visualize this difference.

We can use the entanglement structure diagrams to probe the internal structures of unitary and measurement-only volume law states as a function of system size, L . Fig. 7(a) shows the average entanglement depth and Fig. 7(b) shows the minimal stabilizer weight, n (see Sec. II B). The average is taken over all 500 states for each system size. Although both categories of states show a full entanglement depth, $\sim L$, they differ sharply in their minimal stabilizer weight. This weight grows linearly with system size for volume law states generated by unitary operators while it stays constant for states generated by measurements only. In the states generated by local measurements, the state always contains 2-clusters or 3-clusters. The information stored in the unitary volume law states is more delocalized – extracting any information requires measuring an extensive number of qubits. As is detailed in Appendix B, the large minimal stabilizer

weight makes it expensive to construct entanglement diagrams for the unitary volume law states. Thus we are limited to moderate system sizes, $L \sim 24$ for unitary volume law states due to this increasing complexity.

The entanglement structure diagram enables us to visualize the differences between the entanglement entropy of the unitary and measurement only volume law states. Fig. 5 shows entanglement structure diagrams for a generic unitary and measurement-only volume law state of 20 qubits. The measurement-only state has local sub-clusters that do not have correlations going across the boundary at the middle. These local sub-clusters dilute the long-range spreading of quantum information and reduce the bipartite entanglement entropy. The unitary volume law states have no such local sub-clusters, thus allowing full scrambling of information and maximal entanglement entropy. While both random unitaries and random measurements can produce volume law states, there is more localized information present in the case of measurements.

V. SUMMARY AND OUTLOOK

It is challenging to understand and visualize multipartite entanglement, and the literature contains a number of entanglement measures, each of which are useful in appropriate circumstances [2]. In this paper we introduced a method for characterizing the multipartite entanglement of stabilizer states. It allows us to visualize how quantum information and entanglement is internally distributed among the qubits of a many-body state.

The most immediate application of our technique is understanding the volume law states which are produced in random quantum circuits. None of the traditional entanglement measures are particularly insightful for understanding the properties of these states. Our approach quantifies the way in which information can be extracted from them when clusters of qubits are interrogated. The size and distribution of these clusters helps us identify key differences between volume law states generated by unitary operators vs measurements.

Rather than using a single number to characterize the entanglement, we produce a diagram, which groups the qubits into a hierarchical arrangements of clusters. Each cluster is labeled by an integer which specifies the weight of the smallest stabilizer connecting the elements contained in it. From these diagrams we can extract the entanglement depth, and bound the entanglement entropy across an arbitrary cut. We can also read off the 'minimal stabilizer weight,' which is the weight of the smallest stabilizer.

The entanglement structure diagrams are trivial for many classic stabilizer states. Most states appearing in quantum error correcting codes will have an entanglement structure diagram containing only a single cluster. The GHZ state also has this structure. The 1D cluster state with hard wall boundaries, however, has an entan-

lement structure diagram which reflects the locality of the correlations.

There are several interesting directions that can be explored going forward. In the space of stabilizer states and random quantum circuits, several novel phase transitions and critical states have been found. It would be interesting to resolve structures of critical states and compare different universality classes. We mostly focused on 1D but it is straightforward to extend to higher dimensional states where the spatial structures of correlations can be richer, especially close to criticality [28–31]. Another avenue which we haven’t explored is the evolution of the entanglement structure diagram with time. This would give us important insights and visualization of how quantum information gets scrambled under chaotic dynamics from simple initial states. Although our method is best suited for stabilizer states, it would be fruitful to come up with an efficient method to extend the idea of entanglement structure diagrams to non-stabilizer states.

VI. ACKNOWLEDGEMENTS

This material is based upon work supported by the National Science Foundation under Grant No. PHY-2409403. We would like to acknowledge fruitful discussions with Chaoming Jian during this research’s formative stages.

Appendix A: Algorithmic details for producing the entanglement structure diagrams

Here we extend the discussion from Sec. II, giving a detailed description of how we can construct the entanglement structure diagrams for a stabilizer state, starting from an arbitrary list of stabilizer generators. As described in Sec. II, the key task is to identify w -clusters in each iteration until all qubits have been assigned to decoupled large clusters. Each w -cluster is constructed by identifying sets where subsets of w elements share non-zero total correlations.

In the stabilizer formalism, a pure quantum state of L qubits is described by an $L \times 2L$ binary matrix. The L linearly independent rows encode the Pauli strings which form the stabilizer generators. Each generator can be written in the form, $g = \prod_{i=1}^L X_i^{m_i} Z_i^{n_i}$. The X_i, Z_i are Pauli operators for the i th qubit and m_i, n_i can be 0 or 1. The quantum state is a simultaneous eigenstate of these L linearly-independent stabilizer generators. This representation is not unique, as the state is unchanged by adding any row to another (mod 2).

In order to form our clusters, we must calculate the entanglement entropy of groups of m qubits with the rest of the system. We find this entropy by truncating the stabilizer matrix, keeping only the columns corresponding to these m qubits. The resulting reduced stabilizer matrix (g_m) is an $L \times 2m$ matrix. The entanglement entropy is

given by, $S_m = R - m$ where R is the rank (in modulo 2 arithmetic) of g_m [31]. The value of R can range from m to $2m$. When $R = m$, $S_m = 0$ implying that this m -qubit set is disentangled from the rest of the system. Conversely, if $R > m$, this set is entangled with at least some part of the rest of the system.

This procedure can be used to calculate total correlations of any region A consisting of disjoint groups of qubits, where each group is labeled by an integer i . The total correlations (multipartite mutual information) are defined as, $I_A = \sum_i S_i - S_A$. Here S_A is the entanglement entropy of the entire region A with respect to the rest of the system while S_i is the entanglement entropy of group i with the entire rest of the system.

To calculate our entanglement diagram we begin by placing all of our qubits in a list called `clusters`. Note that in later iterations of the algorithm, each element in `clusters` can contain multiple qubits. We then follow the steps below:

Step 1: Set $n=1$. This integer will keep track of the cluster weight.

Step 2: Calculate entanglement entropy, S of each element in `clusters`. If $S = 0$ for an element, that element is disentangled from the rest of the system. We remove such elements from `clusters` and include them in the final diagram as isolated elements. The list `clusters` now has L_r elements remaining. If $L_r = 0$, the process ends. If $L_r \neq 0$, we proceed to the next step.

Step 3: Increase n by 1.

Step 4: Form all possible combinations/sets of n elements from `clusters`. There are $\binom{L_r}{n}$ of these. Calculate the total correlations, I of each of these n -element sets. If $I = 0$ for all sets, we go back to Step 3 and repeat. If $I \neq 0$ for at least one set, we proceed to Step 5. We refer to the $I \neq 0$ sets as indivisible.

Step 5: Remove the elements of the indivisible sets from `clusters`. Combine the indivisible sets into their disjoint unions, then add these unions back into `clusters` as new elements. These are the n -clusters corresponding to the current iteration of the entanglement structure diagram. Return to Step 1.

The process ends when the list `clusters` is empty and at that point, we have the entire entanglement structure diagram.

Appendix B: Scaling of computation time with system size L

The properties of the many-body state determines the computational time for the entanglement structure diagram. In particular, these diagrams are much more costly to calculate for states which contain clusters with large

w . The reason for this is two-fold: First, given L elements, finding indivisible subsets of w elements requires calculating $\binom{L}{w}$ entropies. Second, each of these entropy calculations requires computing the rank of a $L \times 2w$ matrix, a task whose complexity scales with w .

In Sec. IV we encountered two types of volume law states: Those for which the minimal stabilizer weight, n , is independent of system size, and those for which $n \propto L$. For the former, the entanglement structure diagram can

be calculated in a time which is polynomial in the system size. When $n \propto L$, however, the time scales as $e^{L \ln L}$.

The algorithm to find the entanglement structure diagram itself reveals the complexity and information scrambling of a quantum state. Although volume law states have diverging entanglement entropy, the level of information scrambling can be markedly different depending on whether it is generated by unitary operators or by projective measurements.

[1] R. Horodecki, P. Horodecki, M. Horodecki, and K. Horodecki, Quantum entanglement, *Rev. Mod. Phys.* **81**, 865 (2009).

[2] M. Ma, Y. Li, and J. Shang, Multipartite entanglement measures: a review, *Fundamental Research* <https://doi.org/10.1016/j.fmre.2024.03.031> (2024).

[3] J. Eisert, M. Cramer, and M. B. Plenio, Colloquium: Area laws for the entanglement entropy, *Rev. Mod. Phys.* **82**, 277 (2010).

[4] A. S. Sørensen and K. Mølmer, Entanglement and extreme spin squeezing, *Phys. Rev. Lett.* **86**, 4431 (2001).

[5] O. Gühne, G. Tóth, and H. J. Briegel, Multipartite entanglement in spin chains, *New Journal of Physics* **7**, 229 (2005).

[6] D. A. Meyer and N. R. Wallach, Global entanglement in multiparticle systems, *Journal of Mathematical Physics* **43**, 4273 (2002), https://pubs.aip.org/aip/jmp/article-pdf/43/9/4273/19183190/4273_1.online.pdf.

[7] P. Hyllus, W. Laskowski, R. Krischek, C. Schwemmer, W. Wieczorek, H. Weinfurter, L. Pezzé, and A. Smerzi, Fisher information and multiparticle entanglement, *Phys. Rev. A* **85**, 022321 (2012).

[8] J. Eisert and H. J. Briegel, Schmidt measure as a tool for quantifying multiparticle entanglement, *Phys. Rev. A* **64**, 022306 (2001).

[9] A. Sen(De) and U. Sen, Channel capacities versus entanglement measures in multiparty quantum states, *Phys. Rev. A* **81**, 012308 (2010).

[10] A. Wong and N. Christensen, Potential multiparticle entanglement measure, *Phys. Rev. A* **63**, 044301 (2001).

[11] C. Artiaco, T. K. Kvorning, D. A. Chávez, L. Herviou, and J. H. Bardarson, Universal characterization of quantum many-body states through local information (2024), arXiv:2410.10971 [quant-ph].

[12] T. K. Kvorning, L. Herviou, and J. H. Bardarson, Time-evolution of local information: thermalization dynamics of local observables, *SciPost Phys.* **13**, 080 (2022).

[13] C. Artiaco, C. Fleckenstein, D. Aceituno Chávez, T. K. Kvorning, and J. H. Bardarson, Efficient large-scale many-body quantum dynamics via local-information time evolution, *PRX Quantum* **5**, 020352 (2024).

[14] Y. Li, X. Chen, and M. P. A. Fisher, Quantum zeno effect and the many-body entanglement transition, *Phys. Rev. B* **98**, 205136 (2018).

[15] M. Ippoliti, M. J. Gullans, S. Gopalakrishnan, D. A. Huse, and V. Khemani, Entanglement phase transitions in measurement-only dynamics, *Phys. Rev. X* **11**, 011030 (2021).

[16] D. Gottesman, Stabilizer codes and quantum error correction (1997), arXiv:quant-ph/9705052 [quant-ph].

[17] S. Watanabe, Information theoretical analysis of multivariate correlation, *IBM Journal of Research and Development* **4**, 66 (1960).

[18] A. Kumar, Multipartite quantum mutual information: An alternative definition, *Phys. Rev. A* **96**, 012332 (2017).

[19] D. Bouwmeester, J.-W. Pan, M. Daniell, H. Weinfurter, and A. Zeilinger, Observation of three-photon greenberger-horne-zeilinger entanglement, *Phys. Rev. Lett.* **82**, 1345 (1999).

[20] H. J. Briegel and R. Raussendorf, Persistent entanglement in arrays of interacting particles, *Phys. Rev. Lett.* **86**, 910 (2001).

[21] M. P. Fisher, V. Khemani, A. Nahum, and S. Vijay, Random quantum circuits, *Annual Review of Condensed Matter Physics* **14**, 335 (2023).

[22] S. Choi, Y. Bao, X.-L. Qi, and E. Altman, Quantum error correction in scrambling dynamics and measurement-induced phase transition, *Phys. Rev. Lett.* **125**, 030505 (2020).

[23] Y. Li, X. Chen, and M. P. A. Fisher, Measurement-driven entanglement transition in hybrid quantum circuits, *Phys. Rev. B* **100**, 134306 (2019).

[24] B. Skinner, J. Ruhman, and A. Nahum, Measurement-induced phase transitions in the dynamics of entanglement, *Phys. Rev. X* **9**, 031009 (2019).

[25] A. Lavasani, Y. Alavirad, and M. Barkeshli, Measurement-induced topological entanglement transitions in symmetric random quantum circuits, *Nature Physics* **17**, 342 (2021).

[26] C.-M. Jian, Y.-Z. You, R. Vasseur, and A. W. W. Ludwig, Measurement-induced criticality in random quantum circuits, *Phys. Rev. B* **101**, 104302 (2020), arXiv:1908.08051 [cond-mat.stat-mech].

[27] S. Sang and T. H. Hsieh, Measurement-protected quantum phases, *Phys. Rev. Research* **3**, 023200 (2021).

[28] X. Turkeshi, R. Fazio, and M. Dalmonte, Measurement-induced criticality in (2+1)-dimensional hybrid quantum circuits, *Phys. Rev. B* **102**, 014315 (2020).

[29] P. Sierant, M. Schirò, M. Lewenstein, and X. Turkeshi, Measurement-induced phase transitions in $(d+1)$ -dimensional stabilizer circuits, *Phys. Rev. B* **106**, 214316 (2022), arXiv:2210.11957 [cond-mat.stat-mech].

[30] A. Lavasani, Z.-X. Luo, and S. Vijay, Monitored quantum dynamics and the kitaev spin liquid, *Phys. Rev. B* **108**, 115135 (2023).

[31] V. Sharma, C.-M. Jian, and E. J. Mueller, Subsystem symmetry, spin-glass order, and criticality from random measurements in a two-dimensional bacon-shor circuit, *Phys. Rev. B* **108**, 024205 (2023).

[32] E. Bianchi, L. Hackl, M. Kieburg, M. Rigol, and L. Vid-

mar, Volume-law entanglement entropy of typical pure quantum states, PRX Quantum **3**, 030201 (2022).